Adaptive Robust Self-Balancing and Steering of a Two-Wheeled Human Transportation Vehicle

Shui-Chun Lin · Ching-Chih Tsai · Hsu-Chih Huang

Abstract This paper presents adaptive robust regulation methods for self-balancing and yaw motion of a two-wheeled human transportation vehicle (HTV) with varying payload and system uncertainties. The proposed regulators are aimed at providing consistent driving performance for the HTV with system uncertainties and parameter variations caused by different drivers. By decomposing the overall system into the yaw motion subsystems and the wheeled inverted pendulum, two proposed adaptive robust regulators are synthesized to achieve self-balancing and yaw motion control. Numerical simulations and experimental results on different terrains show that the proposed adaptive robust controllers are capable of achieving satisfactory control actions to steer the vehicle.

Keywords Adaptive control · Wheeled inverted pendulum · Self-balancing · Human transportation vehicle · Yaw motion steering

1 Introduction

Recently, much research has been done on design and applications of self-balancing two-wheeled human transportation vehicles (HTVs), such as Segway™ [1] and PMP

S.-C. Lin
Department of Electronic Engineering, National Chin-Yi University of Technology,
Taichung 41101, Taiwan, Republic of China
e-mail: lsc@ncut.edu.tw

C.-C. Tsai (✉)
Department of Electrical Engineering, National Chung Hsing University,
Taichung 40227, Taiwan, Republic of China
e-mail: cctsai@dragon.nchu.edu.tw

H.-C. Huang
Department of Computer Science and Information Engineering,
Hung Kuang University, Taichung, Taiwan, Republic of China
e-mail: hchuang@sunrise.hk.edu.tw

[2], which have been well recognized as powerful personal transportation vehicles. In particular, these HTVs have been shown useful in the field of neighborhood patrolling and emergency response by police departments [3] and transportation applications [4]. In general, this type of self-balancing two-wheeled HTV can be usually constructed by a synthesis of mechatronics, control techniques and software. For example, the Segway™ is made by quite high-tech and high-quality dedicated components, such brushless servomotor with neodymium magnets, precision gearbox, NiMH batteries, two silica-based wheels, a digital signal processor as a main controller, motor drivers, a gyroscope, and several safety accessories. In contrast to the Segway™, many researchers [5–13] presented low-tech and low-cost self-balancing two-wheeled HTV and claimed that the vehicle can be constructed using the off-the-shelf inexpensive components. Along with the design concepts in [5–13], many human transportation vehicles have been made inexpensive so that they, like bicycles, have highly potential to become prevalent self-balancing two-wheeled vehicles, satisfying human short-distance transportation requirements.

Design and control of self-balancing two-wheeled human transportation vehicles have attracted considerable attention in both industry and academia over the past decade. Sasaki et al. [2] constructed a lightweight self-balancing personal riding-type wheeled mobile platform (PMP), and then achieved the PMP steering control by changing the position of the rider's center of gravity. Grasser et al. [4] presented an unmanned mobile inverted pendulum, called JOE, and Pathak et al. [5] studied the dynamic equations of the wheeled inverted pendulum by partial feedback linearization. Lee et al. [6] investigated the optimal parking of the HTV by a hybrid artificial intelligent approach. Furthermore, Klančar et al. [7] presented a control method for wheeled mobile robots in a linear platoon. However, those HTVs in [2–7] were built for test prototypes, aiming at providing theoretical designs and analytical approaches. The above-mentioned survey reveals that little attention has been paid to design a high-performance but pragmatic controller for this kind of self-balancing HTV.

Although the working principle of these HTVs is similar to that of the wheeled inverted pendulums, these HTVs have more complicated dynamic characteristics than the inverted pendulums do. Moreover, some parameters of the HTV could be altered due to different riders, namely that different riders have different weights, thereby causing some parameter variations on the HTVs. The rider-dependent parameters may deteriorate the controllers which are originally designed to achieving desired control performance. This motivates us to develop model-reference adaptive robust controllers in order to exhibit consistent control performance in the presence of parameter variations. Some adaptive control approaches in [14, 15] and [16] have been documented in some detail. Based upon a reference model which specifies the transient control performance specifications, the synthesis of such a control approach first requires a controller with adjustable parameters, and then finds its parameter adjustment laws via Lyapunov techniques. Huang and Tsai [17] proposed an adaptive robust control for three-wheeled omnidirectional mobile robots; nevertheless, this method can not be applicable to the kind of two-wheeled human transporter.

The objective of the paper is to synthesize two adaptive robust controllers for the human transporter in order to achieve consistent control performance regardless of the riders' weights and parameter variations. In comparison with the state feedback

design by Grasser et al. [4], the key features of the proposed controllers hinge on their adaptivity and robust against static and viscous frictions, and parameter variations. Like the JOE in [4], on basis of the system decomposition into two subsystems: a yaw motion subsystem and an inverted pendulum subsystem, two adaptive robust regulators are designed for not only accomplishing out yaw motion control and self-balancing, but also attaining almost same driving performance for different riders.

The rest of the paper is constructed as follows. Section 2 briefly describes the mathematical modelling of a self-balancing two-wheeled HTV, while Section 3 is devoted to developing the two adaptive robust regulators for self-balancing and steering. In Section 4, particular attention is paid to describe the system structure of the experimental self-balancing HTV and discuss digital implementation issues of the proposed controllers, and then several simulations and experiments are conducted to show the feasibility and effectiveness of the proposed control method. Some conclusions are stated in Section 5.

2 Mathematical Modeling

This section briefly describes a mathematical model of the HTV with two kinds of frictions between the wheels and their motion surface. The first one is the coulomb friction f_c relying on the motion direction of a wheel, namely that $f_c = \mu_c \text{sign}(v)$ where v denotes the speed of the wheel and μ_c represents the coulomb friction coefficient which varies with the property of the surface. The other friction, called the viscous friction, depends on the speed of the wheel and opposite to its moving direction, i.e., $f_v = b_v v$ where b_v represents the coefficient of the viscous friction.

To simplify the derivation of the modeling processing, Table 1 lists all the symbols and their definitions and Fig. 1 illustrates the defined state-space variables for the modeling process. Under the assumption of pure rolling, the mathematical model of the HTV with the friction forces can be modified from Grasser et al. [4] using the

Table 1 Symbols definition

Symbol and unit	Parameter and variable name
$x_{RM}\ [m]$, $v_{RM}\ [m/s]$	Movement position and speed of the Chassis
$\theta_p\ [rad]$, $\omega_p\ [rad/s]$	Pitch angle, pitch angular velocity
$\delta\ [rad]$, $\dot{\delta}\ [rad/s]$	Yaw angle, yaw angular velocity
$C_L\ [N \cdot m]$	Applied torque on left wheel
$C_R\ [N \cdot m]$	Applied torque on right wheel
$J_{RR}\ [kg \cdot m^2]$, $J_{RL}\ [kg \cdot m^2]$	Moment of inertia of the yaw mass with respect to the z axis
$M_{RR}\ [kg]$, $M_{RL}\ [kg]$	Mass of the yaw mass connected to the left and right wheel
$J_{P\theta}\ [kg \cdot m^2]$	Moment of inertia of the chassis with respect to the z axis
$J_{p\delta}\ [kg \cdot m^2]$	Moment of inertia of the chassis with respect to the y axis
$M_P\ [kg]$	Mass of the chassis
$R\ [m]$	Radius of the wheels
$D\ [m]$	Lateral distance between the contact patches of the wheels
$L\ [m]$	Distance between the z axis and the CG of the chassis
b_v, b_θ	Viscous friction coefficients for wheel motion and vehicle rotation

Fig. 1 Illustrations of the
defined state-space variables
in the proposed HTV
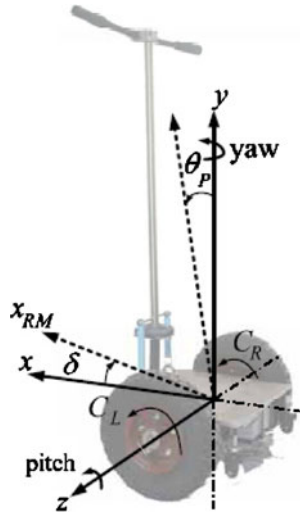
Newtonian mechanism, and the linearized model about the equilibrium of the origin, $x_{RM} = 0$, $\theta_p = 0$ and $\delta = 0$, is then obtained from the following state equation.

$$\dot{\mathbf{x}} = \begin{bmatrix} 0 & 1 & 0 & 0 & 0 & 0 \\ 0 & A_{22} & A_{23} & 0 & 0 & 0 \\ 0 & 0 & 0 & 1 & 0 & 0 \\ 0 & 0 & A_{43} & 0 & 0 & 0 \\ 0 & 0 & 0 & 0 & 0 & 1 \\ 0 & 0 & 0 & 0 & 0 & A_{66} \end{bmatrix} \mathbf{x} + \begin{bmatrix} 0 & 0 \\ B_{21} & B_{22} \\ 0 & 0 \\ B_{41} & B_{42} \\ 0 & 0 \\ B_{61} & B_{62} \end{bmatrix} \begin{bmatrix} C_L \\ C_R \end{bmatrix} + \begin{bmatrix} 0 \\ f_2 \\ 0 \\ f_4 \\ 0 \\ f_6 \end{bmatrix} \tag{1}$$

where the bounded term f_i, $i = 2, 4, 6$, consists of the coulomb friction forces of the two wheels, external disturbances and system uncertainties; the state vector is denoted by $\mathbf{x} = \begin{bmatrix} x_{RM} & v_{RM} & \theta_p & \omega_p & \delta & \dot{\delta} \end{bmatrix}^T$; the parameters in (1) are given as below;

$$A_{22} = \frac{-R^2 \, b_v}{J_R \, \alpha}, \quad A_{23} = -\frac{R^2}{2 J_R} \frac{\gamma}{\alpha \beta}, \quad A_{43} = \frac{\gamma}{J_{P\theta}} \left(1 - \frac{L}{\beta} \right), \quad A_{66} = -\left(\frac{D^2 b_v + 2 b_\delta}{2 J_{P\delta} \, p} \right),$$

$$B_2 = B_{21} = B_{22} = \frac{R}{2 J_R} \left[\frac{1}{\alpha} + \frac{R}{\alpha \beta} \right], \quad B_{23} = B_{24} = \frac{R^2}{2 J_R \alpha}, \quad B_{25} = \frac{R^2}{2 J_R} \frac{1}{\alpha \beta} \cdot \frac{J_{P\theta}}{M_P L},$$

$$B_{45} = \frac{1}{\beta M_p}, \quad B_4 = B_{41} = B_{42} = \frac{1}{J_{P\theta}} \left(\frac{L}{\beta} - 1 \right), \quad B_6 = B_{61} = -B_{62} = \frac{D}{2 p J_{P\delta} R},$$

$$B_{63} = -B_{64} = \frac{D}{2 J_{P\delta} p}.$$

where $p = 1 + \frac{D^2 \cdot (J_R + M_R R^2)}{2 J_{p\delta} R^2}$, $\alpha = \frac{M_R R^2}{J_R} + 1$, $\beta = \frac{J_{P\theta}}{M_P L} + L$, $\gamma = L M_p g$. Using the facts that $B_2 = B_{21} = B_{22}$, $B_4 = B_{41} = B_{42}$, $B_6 = B_{61} = B_{62}$ and utilizing the well-known decoupling matrix developed in [4],

$$\begin{pmatrix} C_L \\ C_R \end{pmatrix} = \begin{pmatrix} 0.5 & 0.5 \\ 0.5 & -0.5 \end{pmatrix} \begin{pmatrix} C_\theta \\ C_\delta \end{pmatrix} \tag{2}$$

the system model (1) is then decomposed into two independent subsystems: one is concerned with the wheeled inverted pendulum subsystem describing by

$$
\begin{pmatrix} \dot{x}_{RM} \\ \dot{v}_{RM} \\ \dot{\theta}_P \\ \dot{\omega}_P \end{pmatrix} = \begin{pmatrix} 0 & 1 & 0 & 0 \\ 0 & A_{22} & A_{23} & 0 \\ 0 & 0 & 0 & 1 \\ 0 & 0 & A_{43} & 0 \end{pmatrix} \begin{pmatrix} x_{RM} \\ v_{RM} \\ \theta_P \\ \omega_P \end{pmatrix} + \begin{pmatrix} 0 \\ B_2 \\ 0 \\ B_4 \end{pmatrix} [C_\theta] + \begin{bmatrix} 0 \\ f_2 \\ 0 \\ f_4 \end{bmatrix}
\tag{3}
$$

and the other is the yaw motion subsystem about the y axis, i.e.,

$$
\begin{pmatrix} \dot{\delta} \\ \ddot{\delta} \end{pmatrix} = \begin{pmatrix} 0 & 1 \\ 0 & A_{66} \end{pmatrix} \begin{pmatrix} \delta \\ \dot{\delta} \end{pmatrix} + \begin{pmatrix} 0 \\ B_6 \end{pmatrix} (C_\delta + \overline{f}_6), \ \overline{f}_6 = f_6/B_6, \left| \overline{f}_6 \right| \le K_{6\max}
\tag{4}
$$

where $A_{66} < 0$ and $B_6 > 0$. From (3) and (4), it is clear that two controllers for C_θ and C_δ can be synthesized independently from each other and combined together to accomplish out the control goals. Worthy of mention is that the controlled torque C_θ is applied to maintain the subsystem at the inclining angle imposed by the rider; hence the torque C_θ is designed via the following simplified equation.

$$
\begin{pmatrix} \dot{\theta}_P \\ \dot{\omega}_P \end{pmatrix} = \begin{pmatrix} 0 & 1 \\ A_{43} & 0 \end{pmatrix} \begin{pmatrix} \theta_P \\ \omega_P \end{pmatrix} + \begin{pmatrix} 0 \\ B_4 \end{pmatrix} (C_\theta + \bar{f}_4), \ \overline{f}_4 = f_4/B_4, \ \left| \bar{f}_4 \right| \le K_{4\max}
\tag{5}
$$

Note that $A_{43} > 0$ and $B_4 < 0$.

Moreover, from (3), it follows that once the pitch angle θ_p has reached a constant angle and $\dot{v}_{RM} = 0$, then the steady-state linear speed of the HTV v_{RMss} will stabilize the vehicle at a constant speed $v_{RMss} = (A_{43}B_2 - B_4 A_{23})\theta_p/(A_{22}B_4)$. This means that when the diver maintains the pitch angle at a specified angle θ_p, the HTV must run at the constant speed v_{RMss} in order to stabilize the vehicle without falling.

On the derived wheeled inverted pendulum with both sensors of inclination and rate gyroscope, the control goal of the subsystem is to maintain the vehicle upright, i.e., to stabilize the inclination angle at origin. Hence, the self-balancing control of the HTV obviously falls into the category of the regulation problem. On the developed yaw motion control subsystem with the potentiometer as the main sensor, the yaw motion control problem can also be reduced to the regulation problem because the potentiometer merely measures the angular error between the angle the rider intended to achieve, and the actual yaw angle of the mobile platform. For this kind of yaw motion control, the reference command is always set to be zero. This simple yaw motion control system avoids the use of a gyroscope, thus circumventing the difficulty of the gyroscope calibration issue.

3 Design of Adaptive Robust Regulators

This section is devoted to developing two adaptive robust regulation laws for C_θ and C_δ to steer the HTV by simultaneously stabilizing it at a desired balancing angle $\theta_P = \theta_{PC} = 0$ and a yaw motion setpoint $\delta_C = 0$ under parameter variations and uncertainties, namely that both controllers are designed to achieve consistent control performance for different riders. Although the dynamics of this self-balancing two-wheeled HTV is nonlinear, both self-balancing and yaw motion controllers can be

independently synthesized by either linearized control technique [4] or nonlinear control approach [5] or. In [5], the partial feedback linearization scheme requires exact system parameters; however, the controller may fail to velocity control and position control due to parameter variations. In [18], an adaptive linearized control method with radial basis function networks was used to achieve self-balancing and yaw motion control in the presence of parameter variations caused by riders' weights. However, the parameter learning of the radial basis function networks in [18] may not converge to their true values due to input signals. To circumvent the shortcoming, the following proposes an adaptive robust PD controller to accomplish out both control goals.

3.1 Adaptive Robust Self-Balancing Regulation

This subsection is devoted to designing an adaptive robust regulator so as to maintain the system at the desired angle $\theta_{PC} = 0$ in the presence of both unknown but constant parameters B_4 and A_{43}, which are caused by different riders. Figure 2 shows the block diagram of the proposed adaptive robust self-balancing control law (6),

$$C_\theta = -\hat{K}_{P\theta}\theta_p - \hat{K}_{D\theta}\omega_p + u_{s1} \qquad (6)$$

where u_{s1} is the robust self-balancing control against weight variations of riders; $\hat{K}_{P\theta}$ and $\hat{K}_{D\theta}$ are estimates of their true parameters $K^o_{P\theta}$ and $K^o_{D\theta}$. In what follows, the design procedure is elucidated for this proposed controller.

Step 1   re-express the subsystem (5) in the subsequent form

$$\dot{\mathbf{X}}_1 = \begin{pmatrix} 0 & 1 \\ A_{43} & 0 \end{pmatrix} \mathbf{X}_1 + \begin{pmatrix} 0 \\ B_4 \end{pmatrix} \left[C_\theta + \overline{f}_4 \right] \qquad (7)$$

where $\mathbf{X}_1 = [\theta_P \ \omega_P]^T$. Assume that the two state variables θ_p and ω_p can be directly available. Then the compatible condition [16] gives the appropriate parameter values of the parameters $K^o_{P\theta}$ and $K^o_{D\theta}$ for perfect model matching

$$K^o_{P\theta} = \left(\omega^2_{n1} + A_{43}\right)/B_4, \quad K^o_{D\theta} = 2\xi_1\omega_{n1}/B_4 \qquad (8)$$

Fig. 2 Block diagram of the proposed adaptive regulator for the decoupled self-balancing subsystem
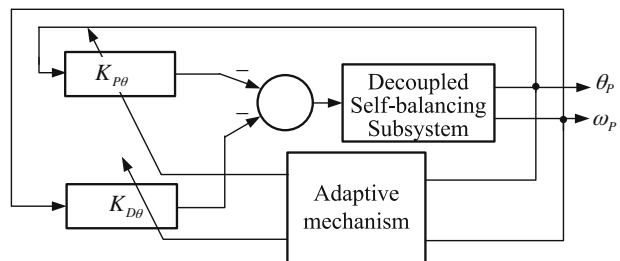
With (8) the subsystem (7) becomes

$$\dot{\mathbf{X}}_1 = \begin{bmatrix} 0 & 1 \\ B_4\left(K_{P\theta}^0 - \hat{K}_{P\theta}\right) - \omega_{n1}^2 & B_4\left(K_{D\theta}^0 - \hat{K}_{D\theta}\right) - 2\xi_1\omega_{n1} \end{bmatrix} \mathbf{X}_1$$
$$+ \begin{bmatrix} 0 \\ B_4\left(u_{s1} + \overline{f}_4\right) \end{bmatrix} \tag{9}$$

Step 2   this step desires to find the rules to adjust the controller's parameters such that $\mathbf{X}_1 \to 0$ i.e., $\theta_p \to \theta_C = 0$ and $\omega_p \to \omega_C = 0$ as $t \to \infty$. In doing so, let the proportional gain error $\tilde{K}_{P\theta}$ be denoted by $\tilde{K}_{P\theta} = K_{P\theta}^0 - \hat{K}_{P\theta}$ and the derivation gain error $\tilde{K}_{D\theta}$ be represented by $\tilde{K}_{D\theta} = K_{D\theta}^0 - \hat{K}_{D\theta}$, thus obtaining $\dot{\tilde{K}}_{P\theta} = -\dot{\hat{K}}_{P\theta}$ and $\dot{\tilde{K}}_{D\theta} = -\dot{\hat{K}}_{D\theta}$. Accordingly, with these two gain errors, (9) turns out

$$\dot{\mathbf{X}}_1 = \mathbf{A}_{m1}\mathbf{X}_1 + \mathbf{\Gamma}_1 \begin{bmatrix} B_4\tilde{K}_{P\theta} \\ B_4\tilde{K}_{D\theta} \end{bmatrix} + \begin{bmatrix} 0 \\ B_4\left(u_{s1} + \overline{f}_4\right) \end{bmatrix} \tag{10}$$

where $\mathbf{A}_{m1} = \begin{bmatrix} 0 & 1 \\ -\omega_{n1}^2 & -2\xi_1\omega_{n1} \end{bmatrix}$ and $\mathbf{\Gamma}_1 = \begin{bmatrix} 0 & 0 \\ \theta_p & \omega_p \end{bmatrix}$. Since $\mathbf{A}_{m1}$ is of the Hurwitz type, there exists a symmetric and positive matrix $\mathbf{P}_1 = \begin{bmatrix} (\xi_1/\omega_{n1}) + \left[\left(\omega_{n1}^2 + 1\right)/4\xi_1\right] & 1/2\omega_{n1}^2 \\ 1/2\omega_{n1}^2 & \left(\omega_{n1}^2 + 1\right)/4\xi_1\omega_{n1}^3 \end{bmatrix}$ such that $\mathbf{A}_{m1}^T\mathbf{P}_1 + \mathbf{P}_1\mathbf{A}_{m1} = -\mathbf{I}$. To show the asymptotical stability of the overall system (10), the following Lyapunov function candidate is proposed as

$$V_1 = \frac{1}{2}\mathbf{X}_1^T\mathbf{P}_1\mathbf{X}_1 + \frac{1}{2B_4\gamma_1} \left[B_4\tilde{K}_{P\theta} \ \ B_4\tilde{K}_{D\theta} \right] \cdot \left[B_4\tilde{K}_{P\theta} \ \ B_4\tilde{K}_{D\theta} \right]^T, B_4\gamma_1 > 0 \tag{11}$$

Note that $B_4 < 0$, $\gamma_1 < 0$. Taking the time derivative of V_1 along its trajectories yields

$$\dot{V}_1 = -\frac{1}{2}\mathbf{X}_1^T\mathbf{X}_1 + \begin{bmatrix} B_4\tilde{K}_{P\theta} \\ B_4\tilde{K}_{D\theta} \end{bmatrix}^T \cdot \left[\mathbf{\Gamma}_1^T\mathbf{P}_1\mathbf{X}_1 + \frac{1}{\gamma_1} \begin{bmatrix} \dot{\tilde{K}}_{P\theta} \\ \dot{\tilde{K}}_{D\theta} \end{bmatrix} \right]$$
$$+ \begin{bmatrix} 0 \\ B_4\left(u_{s1} + \overline{f}_4\right) \end{bmatrix}^T \mathbf{P}_1\mathbf{X}_1 \tag{12}$$

If the parameter adjustment rule is chosen as follows;

$$\mathbf{\Gamma}_1^T\mathbf{P}_1\mathbf{X}_1 + \frac{1}{\gamma_1} \begin{bmatrix} \dot{\tilde{K}}_{P\theta} \\ \dot{\tilde{K}}_{D\theta} \end{bmatrix} = 0$$

which leads to the following parameter adjustment rules

$$\begin{bmatrix} \dot{\hat{K}}_{P\theta} \\ \dot{\hat{K}}_{D\theta} \end{bmatrix} = \gamma_1\mathbf{\Gamma}_1^T\mathbf{P}_1\mathbf{X}_1, \ \gamma_1 < 0 \tag{13}$$

Moreover, if the robust control law is designed as

$$u_{s1} = -K_\theta \, \mathrm{sgn} \left(\theta_P/(2\omega_{n1}^2) + \omega_P \left(\omega_{n1}^2 + 1\right)/\left(4\xi_1\omega_{n1}^3\right)\right), \ K_\theta = K_{2\max} \quad (14)$$

then $\dot{V}_1 = -\mathbf{X}_1^T\mathbf{X}_1/2 \leq 0$ in which $\dot{V}_1$ is negative semidefinite. From (14), Barbalat's lemma implies that $\mathbf{X}_1 \to 0$ as $t \to \infty$. However, the parameter $K_{2\max}$ is constant and unknown and varies with the unknown parameter B_4 such that the control gain K_θ is not easily found. To circumvent the difficulty, another parameter updating law for K_θ is proposed by modifying the Lyapunov equation (11) as

$$V_2 = V_1 + \frac{1}{2B_4\gamma_2}\left(B_4\tilde{K}_\theta\right)^2, \ \tilde{K}_\theta = K_{2\max} - K_\theta, B_4\gamma_2 > 0 \quad (15)$$

which yields the parameter adjustment rule (13) and the following rule

$$\dot{K}_\theta = \gamma_2 \left|\theta_P/(2\omega_{n1}^2) + \omega_P \left(\omega_{n1}^2 + 1\right)/\left(4\xi_1\omega_{n1}^3\right)\right|, \ \gamma_2 < 0 \quad (16)$$

Therefore, the following theorem summarizes the aforementioned result.

Theorem 1 *Let $\gamma_1 < 0$ and $\gamma_2 < 0$. Then the origin of the closed-loop error system, composed of the system (5) and the adaptive robust self balancing controller (6) with the robust control law (14) and the parameter adaptation rules (13) and (16), is globally uniformly bounded. Furthermore, $\theta_p \to \theta_{pc} = 0$, and $\omega_p \to \omega_{pc} = 0$ as $t \to \infty$.*

Remark 1 From the Lyapunov equation $\mathbf{A}_{m1}^T\mathbf{P}_1 + \mathbf{P}_1\mathbf{A}_{m1} = -\mathbf{I}$, one obtains

$$\begin{bmatrix} 0 & -\omega_{n1}^2 \\ 1 & -2\xi_1\omega_{n1} \end{bmatrix}\begin{bmatrix} P_{11} & P_{12} \\ P_{12} & P_{22} \end{bmatrix} + \begin{bmatrix} P_{11} & P_{12} \\ P_{12} & P_{22} \end{bmatrix}\begin{bmatrix} 0 & 1 \\ -\omega_{n1}^2 & -2\xi_1\omega_{n1} \end{bmatrix} = \begin{bmatrix} -1 & 0 \\ 0 & -1 \end{bmatrix}$$

Solving the matrix $\mathbf{P}_1$ attains

$$\mathbf{P}_1 = \begin{bmatrix} (\xi_1/\omega_{n1}) + \left[\left(\omega_{n1}^2 + 1\right)/4\xi_1\right] & 1/2\omega_{n1}^2 \\ 1/2\omega_{n1}^2 & \left(\omega_{n1}^2 + 1\right)/4\xi_1\omega_{n1}^3 \end{bmatrix}$$

It is easy to prove that the matrix $\mathbf{P}_1$ is symmetric and positive-definite for any positive ω_{n1} and ξ_1.

3.2 Adaptive Robust Yaw Motion Regulation

Similar to the previous section, the subsection will be aimed at developing the adaptive robust regulation law for the yaw motion subsystem with unknown parameters A_{66} and B_6 caused by different riders. Figure 3 shows the system structure of the adaptive yaw motion control system under the assumptions of direct measurements of the two variables δ and $\dot{\delta}$. The control aim presented here is to find the following PD-like adaptive control C_δ

$$C_\delta = -\hat{K}_{Pr}\delta - \hat{K}_{Dr}\dot{\delta} + u_{s2} \quad (17)$$

so as to stabilize the yaw motion subsystem. In (17), u_{s2} is the robust yaw motion control law to be determined, and $\hat{K}_{Pr}$ and $\hat{K}_{Dr}$ are estimates of their two true

Fig. 3 Block diagram of
the proposed adaptive
regulator for the decoupled
yaw motion subsystem
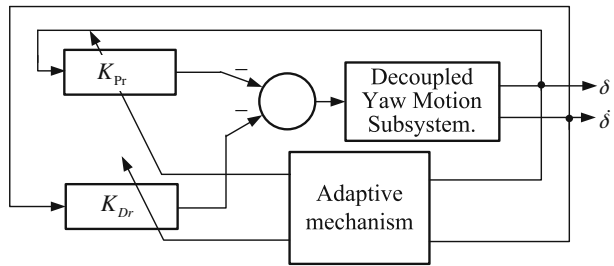
parameters K^o_{Pr} and K^o_{Dr}. The design procedure of this adaptive yaw motion controller is delineated in the following.

Step 1   Rewrite the dynamic equation of the yaw motion subsystem in a state-space model form

$$\dot{\mathbf{X}}_2 = \begin{bmatrix} 0 & 1 \\ 0 & A_{66} \end{bmatrix} \mathbf{X}_2 + \begin{bmatrix} 0 \\ B_6 \end{bmatrix} [C_\delta + \overline{f}_6] \tag{18}$$

where $\mathbf{X}_2 = \left(\delta \; \dot{\delta} \right)^T$. Substituting the control law (17) into the system model (18) gives

$$\dot{\mathbf{X}}_2 = \begin{bmatrix} 0 & 1 \\ B_6 \tilde{K}_{Pr} - \omega^2_{n2} & B_6 \tilde{K}_{Dr} - 2\xi_2 \omega_{n2} \end{bmatrix} \mathbf{X}_2 + \begin{bmatrix} 0 \\ B_6 \left(u_{s2} + \overline{f}_6 \right) \end{bmatrix} \tag{19}$$

where $\tilde{K}_{Pr} = K^0_{Pr} - \hat{K}_{Pr}$; $\tilde{K}_{Dr} = K^0_{Dr} - \hat{K}_{Dr}$; $K^o_{Pr} = \omega^2_{n2}/B_6$, $K^o_{Dr} = (2\xi_2\omega_{n2} + A_{66})/B_6$ and ξ_2 and ω_{n2} respectively represent desired damping ratio and natural frequency of the yaw motion. Note that K^o_{Pr} and K^o_{Dr} are obtained from the compatible condition due to perfect model matching [16].

Step 2   this step is devoted to finding the parameter adjustment rules of the controller such that $\delta \to 0$ and $\dot{\delta} \to 0$ as $t \to \infty$. Thus, equation (19) can be rewritten by

$$\dot{\mathbf{X}}_2 = \mathbf{A}_{m2}\mathbf{X}_2 + \mathbf{\Gamma}_2 \begin{bmatrix} B_6 \tilde{K}_{Pr} \\ B_6 \tilde{K}_{Dr} \end{bmatrix} + \begin{bmatrix} 0 \\ B_6 \left(u_{s2} + \overline{f}_6 \right) \end{bmatrix} \tag{20}$$

where $\mathbf{\Gamma}_2 = \begin{bmatrix} 0 & 0 \\ \delta & \dot{\delta} \end{bmatrix}$ and $\mathbf{A}_{m2} = \begin{pmatrix} 0 & 1 \\ -\omega^2_{n2} & -2\xi_2\omega_{n2} \end{pmatrix}$ is a stability matrix. Because $\mathbf{A}_{m2}$ is of the Hurwitz type, there must exist a symmetric and positive matrix $\mathbf{P}_2 = \begin{bmatrix} (\xi_2/\omega_{n2}) + [(\omega^2_{n2} + 1)/4\xi_2] & 1/2\omega^2_{n2} \\ 1/2\omega^2_{n2} & (\omega^2_{n2} + 1)/4\xi_2\omega^3_{n2} \end{bmatrix}$ such that $\mathbf{A}^T_{m2}\mathbf{P}_2 + \mathbf{P}_2\mathbf{A}_{m2} = -\mathbf{I}$. To prove the asymptotical stability of the closed-loop system (20), one postulates the following Lyapunov function candidate

$$V_3 = \frac{1}{2}\mathbf{X}^T_2 \mathbf{P}_2 \mathbf{X}_2 + \frac{1}{2B_6\gamma_3} \begin{bmatrix} B_6\tilde{K}_{Pr} & B_6\tilde{K}_{Dr} \end{bmatrix} \begin{bmatrix} B_6\tilde{K}_{Pr} & B_6\tilde{K}_{Dr} \end{bmatrix}^T, \; B_6\gamma_3 > 0 \tag{21}$$

Notice that $B_6 > 0$, $\gamma_3 > 0$. Differentiating V_3 with respect to time along its trajectory yields

$$\dot{V}_3 = -\frac{1}{2}\mathbf{X}_2^T\mathbf{X}_2 + \begin{bmatrix} B_6\tilde{K}_{Pr} \\ B_6\tilde{K}_{Dr} \end{bmatrix}^T \left[\mathbf{\Gamma}_2^T\mathbf{P}_2\mathbf{X}_2 + \frac{1}{\gamma_3}\begin{bmatrix} \dot{\tilde{K}}_{Pr} \\ \dot{\tilde{K}}_{Dr} \end{bmatrix} \right]$$

$$+ \begin{bmatrix} 0 \\ B_6\left(u_{s2} + \overline{f}_6\right) \end{bmatrix}^T \mathbf{P}_2\mathbf{X}_2 \qquad (22)$$

If the following parameter adjustment rule is adopted

$$\frac{1}{\gamma_3}\begin{bmatrix} \dot{\tilde{K}}_{Pr} \\ \dot{\tilde{K}}_{Dr} \end{bmatrix} + \mathbf{\Gamma}_2^T\mathbf{P}_2\mathbf{X}_2 = 0$$

which leads to the parameter adaption law.

$$\begin{bmatrix} \dot{\hat{K}}_{Pr} \\ \dot{\hat{K}}_{Dr} \end{bmatrix} = \gamma_3\mathbf{\Gamma}_2^T\mathbf{P}_2\mathbf{X}_2, \ \gamma_3 > 0 \qquad (23)$$

If the robust control law is designed by

$$u_{s2} = -K_\delta \ \mathrm{sgn}\left[\delta/\left(2\omega_{n2}^2\right) + \dot{\delta}\left(\omega_{n2}^2 + 1\right)/\left(4\xi_2\omega_{n2}^3\right)\right], \ K_\delta = K_{6\max} \qquad (24)$$

then $\dot{V}_3 = -\mathbf{X}_2^T\mathbf{X}_2/2 \le 0$, indicating that $\dot{V}_3$ is negative semidefinite. Hence, the use of Barbalat's lemma shows that $\mathbf{X}_2 \to 0$ as $t \to \infty$. Like the argument in Section 3.1, the control gain K_δ is time-varying because the parameter $K_{6\max}$ is constant and unknown, and could vary with the unknown parameter B_6. To circumvent the difficulty, another parameter updating law for K_δ is proposed by modifying the Lyapunov equation (21) as

$$V_4 = V_3 + \frac{1}{2B_6\gamma_4}\left(B_6\tilde{K}_\delta\right)^2, \ \tilde{K}_\delta = K_{6\max} - K_\delta, \ B_6\gamma_4 > 0 \qquad (25)$$

which gives the following rule

$$\dot{K}_\delta = \gamma_4\left|\delta/\left(2\omega_{n2}^2\right) + \dot{\delta}\left(\omega_{n2}^2 + 1\right)/\left(4\xi_2\omega_{n2}^3\right)\right|, \ \gamma_4 > 0 \qquad (26)$$

Before closing this section, one summarizes the main result of this subsection as follows.

Theorem 2 *Assume that $\gamma_3 > 0$ and $\gamma_4 > 0$. Then all the trajectories of the closed-loop system, composed of the system* (20) *and the adaptive robust yaw motion controller* (17) *with the robust control law* (24) *and the parameter adjustment rules* (23) *and* (26), *are globally uniformly bounded. Moreover, $\delta \to 0$ and $\dot{\delta} \to 0$, as $t \to \infty$.*

3.3 Smooth Adaptive Robust Regulators

As motioned previously, both adaptive robust control laws (14) and (24) with their parameter updating rules (16) and (26) have been designed to eliminate the steady-state errors caused by the two uncertain but bounded forces $\overline{f}_4$ and $\overline{f}_6$. However, these robust controllers are composed of two signum functions which

provide switching accelerations for the vehicle at the self-balancing moment. These abrupt and switching forces will cause the rider feel uncomfortable. On the other hand, from the viewpoint of digital implementation, they are difficult to be realized by digital computation devices. Hence, the signum function should be replaced by or approximated by continuous equivalents, for instance, the hyperbolic tangent function which is defined by

$$\tanh(x) = \frac{e^x - e^{-x}}{e^x + e^{-x}}, \; x \in R \tag{27}$$

The hyperbolic tangent function has been shown powerful in achieving the same control goal without chattering phenomena [19]. In the subsection, this hyperbolic tangent function is employed to carry out smooth adaptive robust controls instead of both original signum functions. Thus, with two positive real numbers a and b, the robust control law (14) is then modified by

$$u_{s1} = -K_\theta \tanh((a + bt)s_1), s_1 = \theta_P/(2\omega_{n1}^2) + \omega_P \left(\omega_{n1}^2 + 1\right)/\left(4\xi_1\omega_{n1}^3\right) \tag{28}$$

and the robust control law (24) is changed to

$$u_{s2} = -K_\delta \tanh((a + bt)s_2), s_2 = \delta/(2\omega_{n2}^2) + \dot{\delta} \left(\omega_{n2}^2 + 1\right)/\left(4\xi_2\omega_{n2}^3\right) \tag{29}$$

Note that both smooth adaptive robust controllers use the hyperbolic tangent function instead of the signum functions, in order to avoid possible chattering phenomena. When the signum function is replaced by the hyperbolic tangent function, the stability issue of the proposed smooth controller can be similarly proven by using the same argument of the method presented in [19].

## 4 Simulations, Experimental Results and Discussion

In this section, three simulations and two experiments are performed to investigate the effectiveness and performance of the proposed self-balancing and yaw motion regulators. The first two simulations are conducted to verify the feasibility and effectiveness of the proposed control methods, and the third simulation is used to show the superiority of the proposed controllers in comparison with the state feedback controllers in [5]. The first experiment is conducted to examine the performance and applicability of the proposed adaptive self-balancing regulators for two riders with weights of 85 kgw and 60 kgw, respectively. The second experiment attempts to investigate the usefulness of the proposed adaptive yaw motion regulator for the same two riders.

4.1 Brief Description of Experimental Self-Balancing HTV

4.1.1 Mechatronic Design

Figure 4 displays the photograph of the laboratory-built personal self-balancing HTV with two differential driving wheels. This vehicle is composed of one foot plate, two 24V DC servomotors with gearbox and two stamped steel wheels with 16-in. tires, two 12-V sealed rechargeable lead-acid batteries in series, two motor drives, one digital signal processor (DSP) board TMS 320LF240 from Texas Instrument used to implement the controller, one handle-bar with a potentiometer as a yaw motion

Fig. 4 The experimental
self-balancing two-wheeled
HTV: **a** front view;
b bottom view
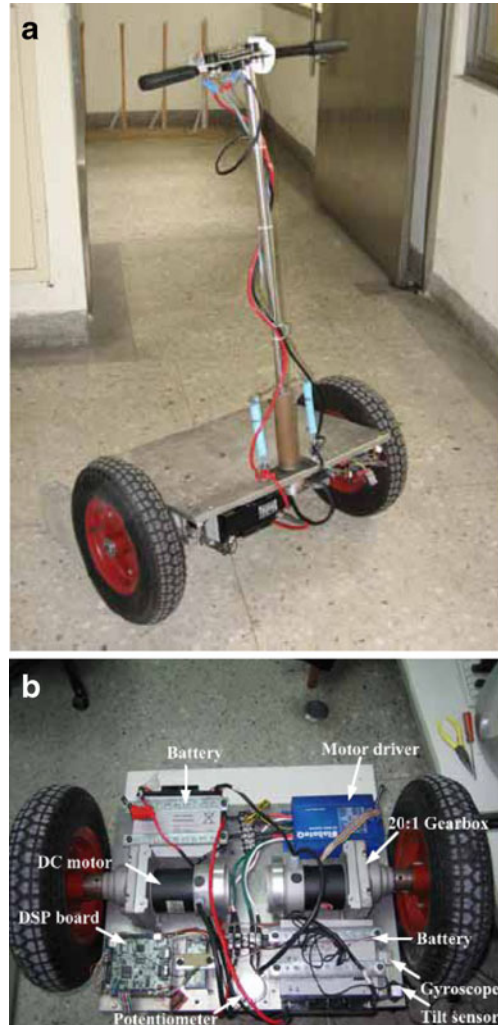
position sensor, one gyroscope and one tilt sensor. The two motor drives use dual
H-bridge circuitry to deliver PWM-based power to drive the two DC servomotors.
Sending PWM signals to the H-bridge circuit, the DSP controls linear speed and
yaw motion of the HTV as well as maintains the self-balancing of the HTV. The
used piezoelectric vibrating gyroscope is the mode1 ENV-05H-02 Gyrostar supplied
by Murata electronics, in which the vibrating prism inside the gyroscope is used as
the sensing element by measuring the phase differences of surface acoustical waves
across the prism. The signal from the Gyrostar ranges from 0 VDC to 5 VDC, with
the output 2.5 VDC at zero angular velocity. This gyroscope is adopted to measure
the pitch angle rate of the HTV, and the title sensor CXTA02 from Crossbow uses
a micro-machined acceleration sensing element with a DC response to measure
inclination relative to gravity. The tilt sensor measures the pitch angle and its
output is an offset voltage plus the voltage response proportional to the amount of

Fig. 5 Block diagram of the overall HTV control structure
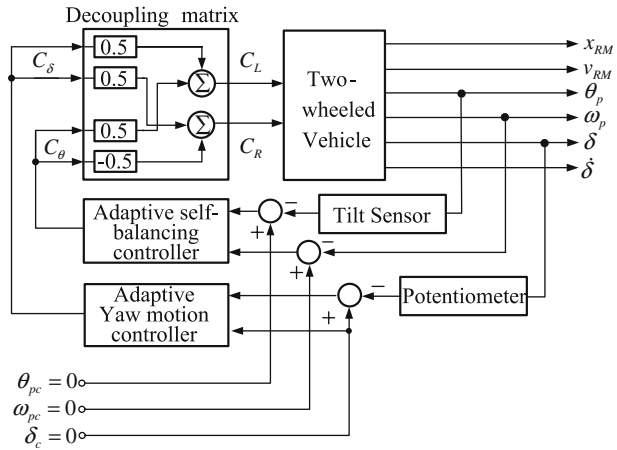
gravity measured by the sensor. Note that voltage response of the sensor CXTA02 is proportional to the sine of the tilt angle.

4.1.2 Control Architecture

The block diagram of the control system for the transporter is shown in Fig. 5, which is equipped with a tilt sensor, a gyroscope, a potentiometer, an adaptive self-balancing regulator and an adaptive yaw motion regulator. Figure 6 shows the system structure of the entire HTV control system. The DSP controller with built-in A/D converter is responsible for executing the control algorithms including yaw motion control and self-balancing control. The feedback signals from the gyroscope and tilt sensors are utilized via the controller to maintain the human body on the footplate without falling. Note that the two first-order filters can be employed to remove the unwanted signal in both the pitch angle rate reading ω_P from the gyroscope and the pitch angle reading θ_P from one tilt sensor, thus reducing high-frequency noise effects. Worthy of mention is that the filtering method proposed in [18] can be employed to obtain more accurate estimates of ω_P and θ_P.
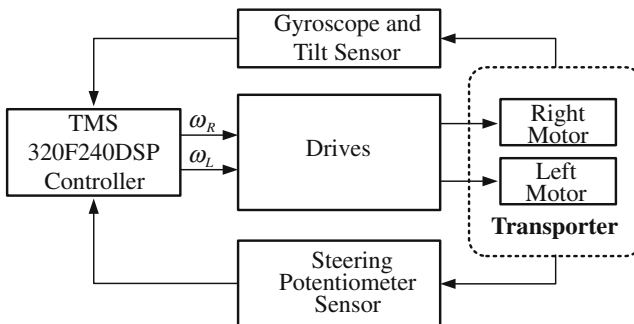

Fig. 6 Block diagram of control Signals in the entire HTV control system

Table 2 Parameters for computer simulations

Parameters	Adaptive robust self-balancing controller	Adaptive robust yaw motion controller
A_{43}	7	–
A_{66}	–	−0.04
B_4	−0.0102	–
B_6	–	0.57
ω_n	10	10
η	0.707	0.707
γ	−4.	2

4.2 Simulation Results and Discussion

The self-balancing HTV with the proposed adaptive control laws (6) and (17) was simulated on a digital computer using Matlab package. The parameters given in Table 2 are adopted in this simulation. The simulations examined the performance of the proposed regulators for a rider with an unknown weight and a given external force applied to the HTV. Figures 7b and 8b respectively depict the output responses of the proposed yaw motion and self-balancing regulators when left and right yaw motion commands and then forward and backward moving command were applied to the HTV, as shown in Figs. 7a and 8a. The results in Figs. 7b and 8b indicate that the proposed regulators are capable of giving satisfactory regulation performance for a rider with unknown weight and given external disturbance.

For showing the superiority of the proposed controller, the third simulation is conducted for the self-balancing two-wheeled HTV using the state-feedback controllers proposed in [5]. Figure 9 compares the simulation results of the pitch angle responses for the state-feedback controller and the proposed adaptive controller. As shown in
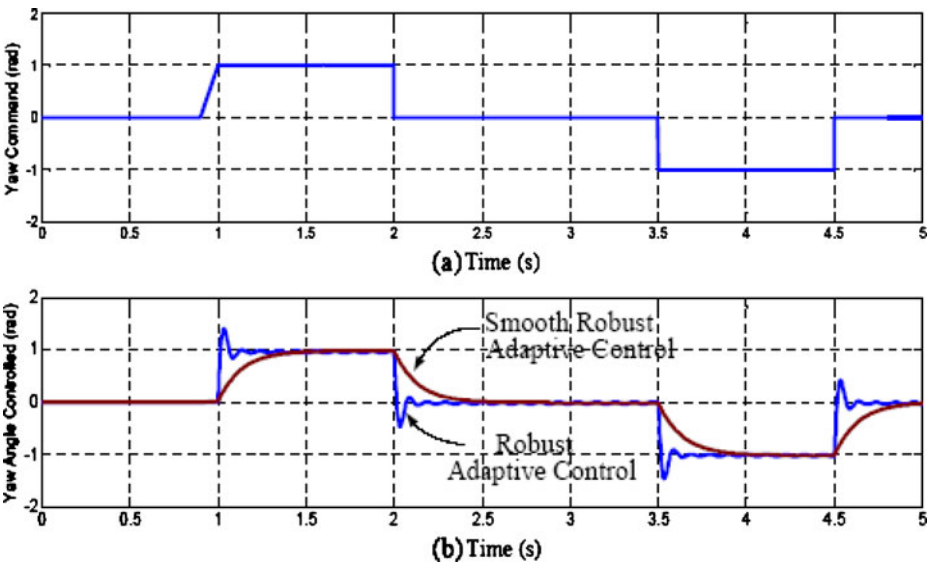

Fig. 7 Regulation performance for the yaw motion profile: **a** yaw motion tracking; **b** simulated yaw-angle output
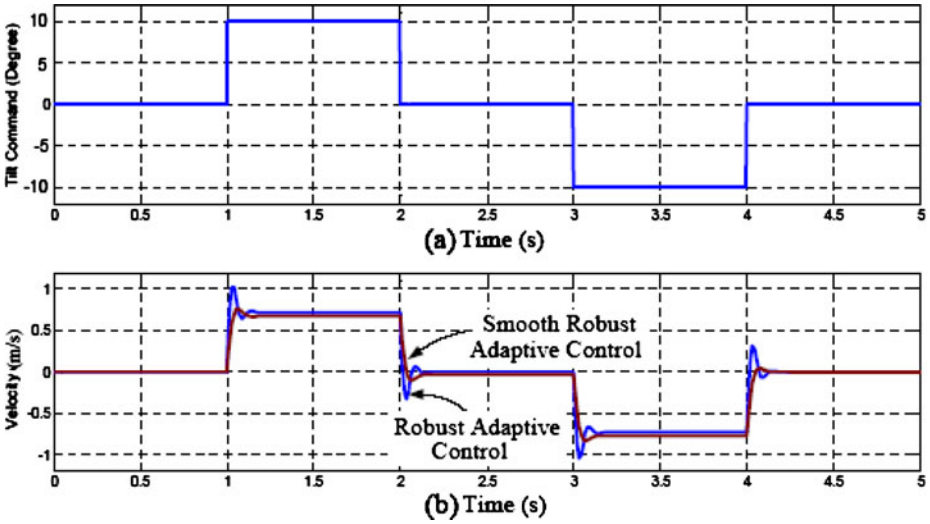
Fig. 8 Regulation performance for the motion profile: **a** tilt command; **b** simulated tilt-angle output

Fig. 9, the proposed adaptive self-balancing controller has a faster transient response with a smaller error of 0.0004 rad/s than the state-feedback controller does. Figure 10 presents the yaw angle control performance for the state-feedback controller and the proposed yaw controller. The results in Fig. 10 clearly indicate that the proposed adaptive yaw controller has a better response than the state-feedback controller does. The results in Figs. 9 and 10 show that the proposed controllers outperform the state-feedback controllers.
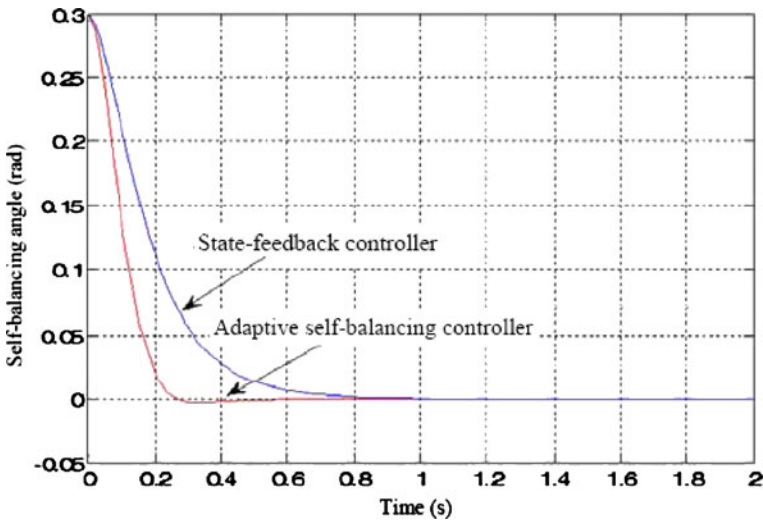
Fig. 9 Comparison between both simulation results of the pitch angle tracking for the state-feedback controller and the smooth adaptive self-balancing controller
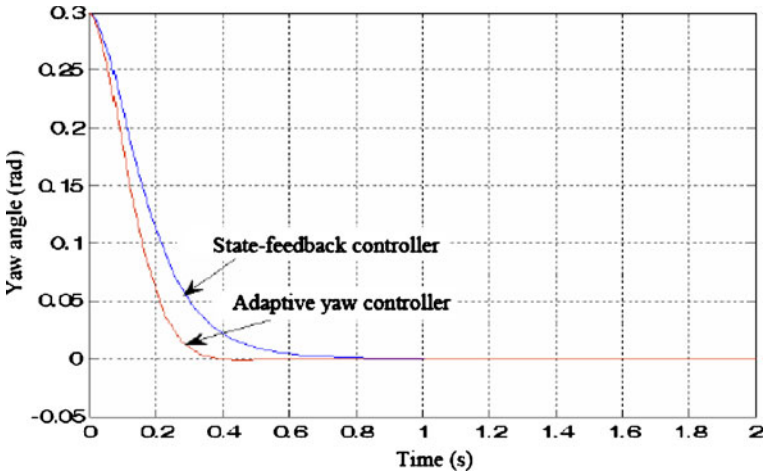
Fig. 10 Comparison between both simulation results of the yaw angle tracking for the state-feedback controller and the smooth adaptive yaw motion controller

4.3 Digitalization of the Proposed Adaptive Regulators

Before experimentation, the two proposed adaptive regulators with the parameter update laws, (6) and (17) must be digitalized such that they can be executed by the DSP-based controller in real time. These can be easily done by using backward difference and bilinear transformation. For the adaptive robust self-balancing regulator, its digital equivalent is given by

$$C_\theta(k) = -\hat{K}_{P\theta}(k)\theta_p(k) - \hat{K}_{D\theta}(k)\left(\frac{\theta_p(k) - \theta_p(k-1)}{T}\right) + u_{s1}(k) \qquad (30)$$

and

$$\begin{bmatrix} \hat{K}_{P\theta}(k) \\ \hat{K}_{D\theta}(k) \end{bmatrix} = \begin{bmatrix} \hat{K}_{P\theta}(k-1) \\ \hat{K}_{D\theta}(k-1) \end{bmatrix}$$

$$+ \frac{\gamma_1 T}{2}\left(\gamma_1 \mathbf{\Gamma}_1^T(k-1)\mathbf{P}_1\mathbf{X}_1(k-1) + \mathbf{\Gamma}_1^T(k-1)\mathbf{P}_1\mathbf{X}_1(k-1)\right), \gamma_1 < 0$$

$$(31)$$

Repeating the same procedure gives the digitalization of the adaptive robust yaw motion regulator as follows;

$$C_\delta(k) = -\hat{K}_{Pr}(k)\delta(k) - \hat{K}_{Dr}(k)\left(\frac{\delta(k) - \delta(k-1)}{T}\right) + u_{s2}(k) \qquad (32)$$

and

$$\begin{bmatrix} \hat{K}_{Pr}(k) \\ \hat{K}_{Dr}(k) \end{bmatrix} = \begin{bmatrix} \hat{K}_{Pr}(k-1) \\ \hat{K}_{Dr}(k-1) \end{bmatrix} + \frac{\gamma_2 T}{2}\left(\mathbf{\Gamma}_2^T(k-1)\mathbf{P}_2\mathbf{X}_2(k-1) + \mathbf{\Gamma}_2^T(k)\mathbf{P}_2\mathbf{X}_2(k)\right), \gamma_2 > 0$$

$$(33)$$

The speed commands for the right-side and left-side motors of the HTV are respectively computed by the following two torque-to-speed relations

$$\omega_L(k) = \omega_L(k-1) + \frac{T \cdot (C_\theta(k) + C_\delta(k))}{2J_L} \tag{34}$$

and

$$\omega_R(k) = \omega_R(k-1) + \frac{T \cdot (C_\theta(k) - C_\delta(k))}{2J_R} \tag{35}$$

Note that J_L and J_R are constant moments of inertia of the two motors.

For implementation of the two adaptive robust regulation algorithms, the following steps are presented in order to avoid the computation delay problem.

Step 1   Measure signal from the tilt sensor and the potentiometer via the analog-to digital conversion of the DSP-based controller.
Step 2   Compute $C_\theta(k)$ and $C_\delta(k)$ from (30) and (31).
Step 3   Calculate both motors' speed commands from (34) and (35).
Step 4   Output the motor's speed PWM commands.
Step 5   Estimate the controllers $\hat{K}_{P\theta}(k)$ and $\hat{K}_{D\theta}(k)$ from (31) and the controllers $\hat{K}_{Pr}(k)$ and $\hat{K}_{Dr}(k)$ from (33).
Step 6   Wait for next sampling instant, and go to Step 1.

Notice that the aforementioned real-time algorithm is synthesized based on the principle that the control signals must be outputted by 10% time of each sampling interval, and the remaining time is employed to update the controller parameters of the two adaptive regulators.

Fig. 11 The moving HTV ridden by the first rider (185 cm/87 kg): **a** moving forward; **b** moving backward
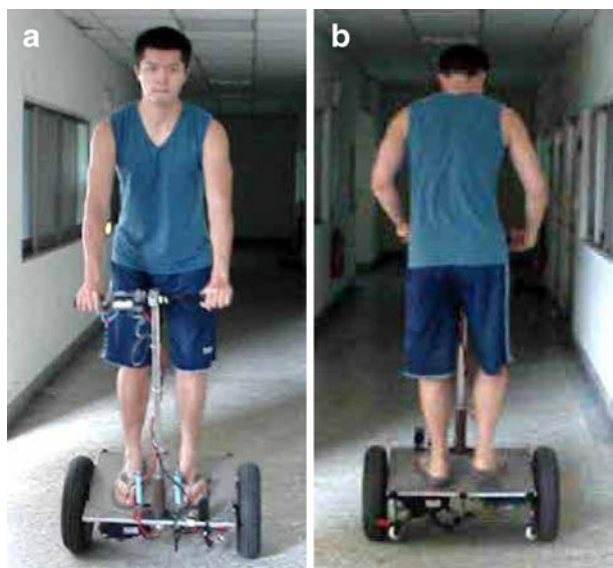
Fig. 12 The moving HTV
ridden by the second rider
(165 cm/60 kg): **a** moving
forward; **b** moving backward

4.4 Experimental Results of Adaptive Self-Balancing and Yaw Motion Regulation

This following subsection describes experimental results of the proposed adaptive self-balancing and yaw motion regulators whose real-time control algorithm was implemented by standard C language. The relevant parameters used for both experiments are $\gamma_1 = -4.3$, $\gamma_3 = 2.34$, the damping ratio ξ_1 and the natural frequency ω_{n1} for self-balancing are 0.707 and 5 rad/s, and the damping ratio ξ_2 and the natural

Fig. 13 The turning HTV
ridden by a rider
(185 cm/87 kg): **a** turning left;
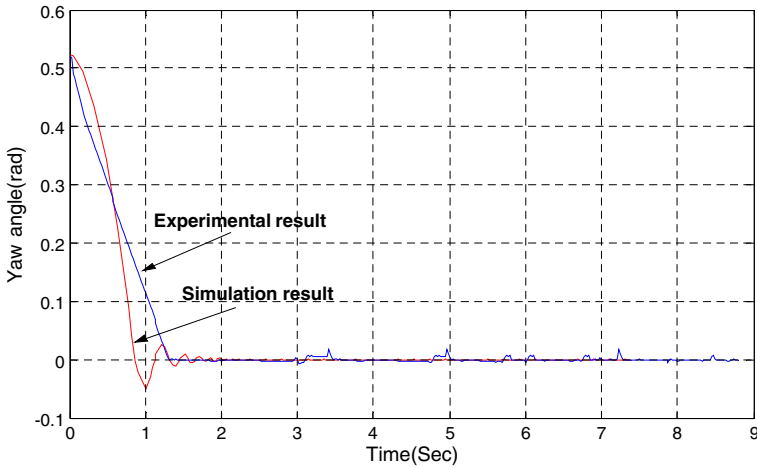**b** turning right

Fig. 14 Experimental yaw response of the smooth adaptive yaw controller for both riders

frequency ω_{n2} for yaw motion are 0.707 and 10 rad/s, respectively. Moreover, both matrices $\mathbf{P}_1$ and $\mathbf{P}_2$ are given by

$$\mathbf{P}_1 = \begin{bmatrix} 9.335 & 0.02 \\ 0.02 & 0.0735 \end{bmatrix}, \quad \mathbf{P}_2 = \begin{bmatrix} 35.785 & 0.005 \\ 0.005 & 0.03536 \end{bmatrix} \tag{36}$$

The PWM control signals are limited to 0% and +100%. Extensive experiments were conducted to verify the performance of the HTV with the proposed real-time regulation algorithm. Figures 11 and 12 depict the moving HTV ridden by the two riders while the HTV was moving in a straight line on smooth floor. The results in Fig. 13 illustrates turning behavior of the turning HTV with the two proposed
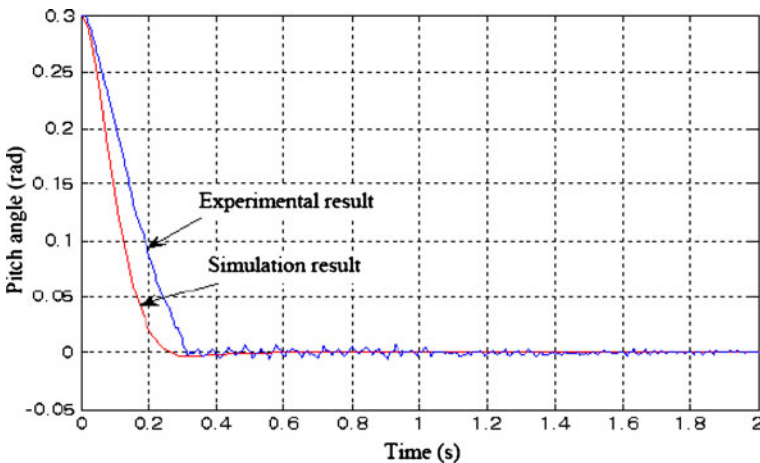

Fig. 15 Experimental pitch response of the smooth adaptive self-balancing controller for both riders

adaptive regulators. Figures 14 and 15 the experimental and simulation results of the two proposed controllers for both riders. These results have exemplified the effectiveness of the proposed controller for the two-wheeled human transportation vehicle. Through those experimental results, the proposed real-time adaptive regulation algorithm has been shown capable of giving satisfactory performance for the HTV, and the performance of the controller HTV has not been affected by different riders.

5 Conclusions

This paper has presented two adaptive robust regulators for a two-wheeled human transportation vehicle which can be decoupled into the wheeled inverted pendulum and yaw motion subsystems. Both adaptive robust regulators have been designed such that all the nonzero initial states converge to zero with desired transient responses. Two sets of parameters adjustment rules have been derived based on the Lyapunov stability theory. Through simulations and experimental results, the transporter with both proposed two regulators has been shown capable of giving satisfactory riding performance for different riders. An interesting topic for future research would be to develop a nonlinear model and a nonlinear adaptive control method for the two-wheeled human transportation vehicle.

References

1. Lin, S.C., Tsai, C.C.: Development of a self-balancing human transportation vehicle for the teaching of feedback control. IEEE Trans. Ed. **52**(1), 157–168 (2009)
2. Sasaki, M., Yanagihara, N., Matsumoto, O., Komoriya, K.: Steering control of the personal riding-type wheeled mobile platform (PMP). In: Proc. IEEE International Conference on Intelligent Robots and Systems, pp. 1697–1702 (2005)
3. Petty, R.D.: Transportation technologies for community policing: a comparison. In: Proc. IEEE ISTAS/CPTED'03, pp. 33–38 (2003)
4. Grasser, F., Arrigo, A.D., Colombi, S.: JOE: a mobile, inverted pendulum. IEEE Trans. Ind. Electron. **49**(1), 107–114 (2002)
5. Pathak, K., Franch, J., Agrawal, S.K.: Velocity and position control of a wheeled inverted pendulum by partial feedback linearization. IEEE Trans. Robot. Autom. **21**(3), 505–513 (2005)
6. Lee, C.K., Lin, C.L., Shiu, B.M.: Autonomous vehicle parking using hybrid artificial intelligent approach. J. Intell. Robot. Syst. **56**(3), 319–343 (2009)
7. Klančar, G., Matko, D., Blažič, S.: Wheeled mobile robots control in linear platoon. J. Intell. Robot. Syst. **54**(5), 709–731 (2009)
8. Bapiraju, B., Srinivas, K.N., Prem Kumar, P., Behera, L.: On balancing control strategies for a reaction wheel pendulum. In: Proc. IEEE INDICON'04, pp. 199–204 (2004)
9. Browning, B., Rybski, P.E., Searock, J., Veloso, M.M.: Development of a soccer-playing dynamically-balancing mobile robot. In: Proc. IEEE ICRA'04, vol. 2, pp. 1752–1757 (2004)
10. Salerno, A., Angeles, J.: The control of semi-autonomous two-wheeled robots undergoing large payload-variations. In: Proc. ICRA'04, vol. 2, pp. 1740–1745 (2004)
11. Ou, Y., Xu, Y.: Convergence analysis for a class of skill learning controllers. In: Proc. IEEE ICRA'04, vol. 3, pp. 2653–2658 (2004)
12. Searock, J., Browning, B., Veloso, M.: Turning Segways into soccer robots. In: Proc. IEEE Int. Con. Intelligent Robots Syst, vol. 1, pp. 1029–1034 (2004)

13. Fleischer, J., Szatmary, B., Hutson, D., Moore, D., Snook, J., Edelman, G.M., Krichmar, J.: A neurally controlled robot competes and cooperates with humans in Segway soccer. In: Proc. IEEE International Conference, ICRA '06, vol. 3, pp. 3673–3678 (2006)
14. Anderson, R.T., Chowdhary, G., Johnson, E.N.: Comparison of RBF and SHL neural network based adaptive control. J. Intell. Robot. Syst. **54**(1–3), 183–199 (2009)
15. Khalil, H.K.: Nonlinear Systems, 3rd edn. Prentice Hall, New York (2002)
16. Astrom, K.J., Wittenmark, B.: Adaptive Control, 2nd edn. Addison Wesley, New York (1995)
17. Huang, H.C., Tsai, C.C.: Adaptive robust control of an omnidirectional mobile platform for autonomous service robots in polar coordinates. J. Intell. Robot. Syst. **51**(4), 439–460 (2008)
18. Tsai, C.C., Huang, H.C., Lin, S.C.: Adaptive neural network control of a self-balancing two-wheeled scooter. IEEE Trans. Ind. Electron. **57**(4), 1420–1428 (2010)
19. Huang, C.I.: Sliding mode control of motion platform and human-perception-systems based washout filter design for virtual reality simulation. Ph.D. Dissertation, Department of Electrical Engineering, National Taiwan University (2007)